Analysis of Brush Seal Interaction with Steam Turbine Rotor-Shafts

Nonso U. Omenife[1,2], Dawood A. Desai[1], Regan K. Dunne[1]

[1]Department of Mechanical and Mechatronics Engineering. Tshwane University of Technology, Pretoria South Africa.
[2]Department of Mechanical/ Production Engineering, Nnamdi Azikiwe University. Awka, Anambra state Nigeria.

Abstract

High-speed turbines are a major source for power production. They utilize high pressure and temperature fluid flow. Sealing of these machines to decrease the flow losses has been a major engineering challenge since the inception of steam turbines. From an engineering viewpoint, seals are used to introduce friction in the fluid flow path. This reduces the flow leakage. Improved seal performance offers substantial opportunities for turbine performance. Reduced leakages in steam turbines can lead to greater efficiency and power output. They can also allow tighter control of turbine secondary flows. However, sealing these machines is a major challenge. There are several seal locations on a steam turbine that have significant performance derivatives. These include the interstage shaft packing, the end packing, and the bucket tip seals. Brush seals are ideal for these locations because they can reduce the flow losses. This study analysed the efficiency of the steam turbine by using ANSYS APDL. It assessed the leakage performance of the brush seal for different cases and geometries. It also used porous medium modelling of the bristle pack to provide insight for designers. The outputs of interest were the rotor-shaft temperature and the efficiency of the entire turbine with the brush seal.

Keywords: *Brush seal, steam turbine, Ansys, sealing.*

1. Introduction

In recent years, many efforts have been focused on numerically investigating the leakage flow characteristics of brush seals. For example, Qiu B, Li J, and Yan X simulated the leakage flow in the brush seals by the non-darcian porous medium approach [1]. [2] Ma et al employed the modified bulk porous medium approach to evaluate the effects of the front and backing plate configurations on the flow fields of brush seals. Zhang et al discussed the leakage flow of two kinds of brush seals with the porous medium model [3].

A majority of the studied literature analysed the leakage flow characteristics of brush seals based on the simplified porous medium model and did not use fluid-solid interaction (FSI). Practical operation and studies have shown that the deflection of flexible bristle packs due to flowing pressure influences the flow characteristics. Under this circumstance, FSI analysis is implemented by two-way coupling iterative algorithm. However, the relationship between rotordynamic coefficients and the geometry of a brush seal is explored by performing a brush seal porous media model analysis and fluid-solid coupling model analysis that will numerically analyse a typical single-stage brush seal, for different geometries and operating conditions.

The objective of this paper is to present the investigations of brush seals comprising of the flow field characteristics and the effect of structural parameters on the leakage characteristic. The sealing brushes are made into spring-backed sealing portions, and it is for the steam and gas turbine machines which are used in the applications of the sealing shafts. The sealing brushes are made into spring-backed sealing portions, for the steam and gas turbine machines which are used in the

applications of the sealing shafts. A single ring of the sealing fins consists of six to eight portions, more sealing brush components are present, and each portion has many sealing fins. If the sealing brush is not able to work, it may serve as a backup solution, according to Hildebrandt et al [4].

In this study attachment of brush seals to the rotor-shaft was evaluated by the replacement of mechanical seals with the floating brush seal, and an exploratory study that enhances sealing technology, by determining brush seal leakages through brush seal analysis. A brush seal contains many thousands of fine wires, which touch the rotor, forming an effective barrier to steam flow, whilst retaining the ability to deflect during shaft excursions and thermal movements without permanent loss of sealing efficiency.

2. Materials and Methods

2.1. Materials

The brush seal is composed of a pack of fine bristle diameters which is compressed between the front plate and backing plate. It is made of Haynes 25 fibres that have diameters between 0.05- and 0.15-mm. Fibre density ranges from 38100 to 63500 fibres per mm of seal circumferences. Haynes 25 is a cobalt-based super alloy that has suitable resistance to high temperature, oxidation, and deformation. It is shaped and manufactured by traditional methods. The Main properties of Haynes 25 are illustrated in table 1. However, this study aims to provide the theoretical basis for designing a brush seal structure that is as simple as possible, as shown in Figure 1.
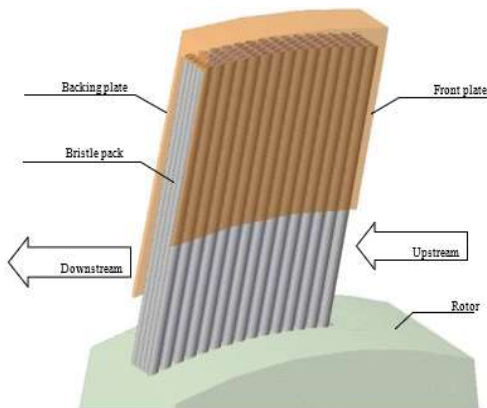

Figure 1. Schematic diagram of brush seal structure [5].

Table 1. Haynes 25 -10% cold worked, material properties at room temperature.

Lay angle (0)	45^0
Diameter of bristle (d)	0.127 mm
Bristle pack width (t)	1.27 mm
Bristle free length (H_b)	23.75 mm
Fence height (H_f)	1.78 mm
Porosity of brush seal	18%
Materials	
Bristles	Haynes 25

The brush seal is mounted between the rotor and stator. Figure 2 illustrates the brush seal structure and design parameters. (BH) refers to free bristle height, (FH) shows fence height, and rotor radius is denoted by (R). A Brush seal is placed between low-pressure and high-pressure regions around rotating shafts. Fluid moves in the axial direction from the upstream region which has higher pressure to the downstream region which has lower pressure. Front-plate clamps hold the bristles in place while the backing plate is used for mechanical reinforcement under pressure load. The Brush seal is fixed at the stator typically with a small interference on the rotor surface as shown in Figure 2. While the seal is in a static member, bristles make contact with the rotor at an acute angle. This angle is between the rotor surface normal and bristles direction is called "Cant" angle or lay angle.
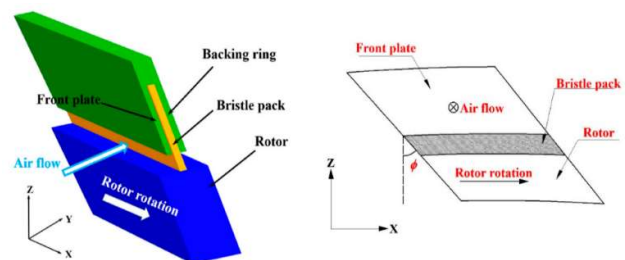

Figure 2. Brush seal structure [6].

The Cant angle allows bristles to bend and deform when interference occurs during rotor excursions, which significantly reduces contact severity. The Cant angle is designed mostly between 35º and 55º. Since a brush seal is applied to reduce leakage, a mass flow rate that moves through the brush seal becomes a major parameter to

determine the performance of the design. Fence height is the radial distance between backing plate inner radius and rotor surface, and free bristle height is defined as the radial distance between pinch point and seal inner radius.

2.2. Methodology

This study analysed the effect of various factors on the performance of a brush seal. These factors include the temperature and viscosity of lubricants, rotor speed, pressure ratio, clearance, and the cavity size of the sealing structure. The study also explored the relationship between rotordynamic coefficients and the geometry of a brush seal. To do this, the study performed two types of numerical analysis: a brush seal porous media model analysis and a fluid-solid coupling model analysis using Ansys APDL. These analyses used a typical single-stage brush seal for different geometries and operating conditions.

3. Brush Seal Effective Clearance Calculation

Effective clearance values provide an important metric to compare brush seal leakage performance for different cases and geometries. The one-dimensional mass flow equation for the calculation is given below, and Figure 3 illustrates the leakage flow pattern across the clearance of the brush seal.
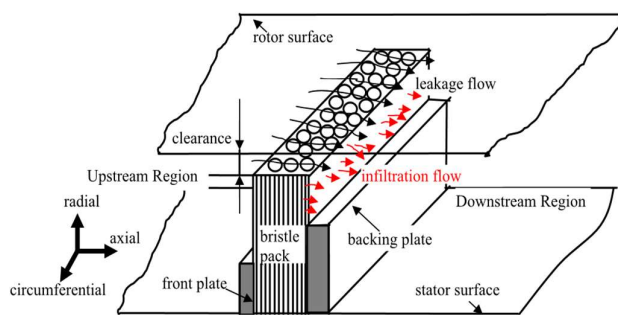

Figure 3. Illustrates the leakage flow pattern across the clearance of the brush seal [7].

The one-dimensional mass flow equation is given as

$$\dot{m} = pAV \tag{1}$$

where, $\dot{m}$ is mass flow rate, ρ is density, V is velocity and A is the area of the flow. The following flow function (FF) is defined in terms of total pressure, total temperature, and specific heat ratio:

$$FF = \frac{\dot{m}\sqrt{T_T}}{P_T\,A_{eff}}\,; \tag{2}$$

Then effective clearance of the brush seal is defined as,

$$CL_{eff=\frac{\dot{m}\sqrt{T_T}}{\pi DPT^{FF}}}\,; \tag{3}$$

The expression of flow function varies according to the pressure ratio and the ratio of specific heat, where P is downstream static pressure. Effective clearance values provide an important metric to compare brush seal leakage performance for different cases and geometries by Reggentin and Friedrichs [8].

3.1. Rotordynamic characteristics of a single brush seal

In the dynamic sealing of steam turbines, the brush seal technology gains an ever-broader application. Using brush seals with their advantageous leakage characteristics in place of conventional labyrinth seals is one of the cost-effective ways of meeting the current demands for higher efficiency and lower environmental impact of new and retrofitted turbomachinery units. To overcome the abrasive nature and undesired structural effects of bristles, novel materials have been studied. However, Haynes 25 is still preferred for steam turbine brush seals where-high temperature tolerance and resilient bristles are needed. As suggested by Yunseok et al, the dynamic characteristics of tribo-elements have been utilized to analyse a given rotordynamic system [9]. Additional stiffness or damping could be the source of destabilizing force, inducing the steam whirl.

In addition, thermal instability, such as the Newkirk effect, can appear due to unavoidable frictional heating resulting from contact between the bristles and rotor. The stiffness of the brush seal was extracted through the circumferential pressure distribution between the bristle packs, and owing to the blow-down effect, the dynamic characteristics of the brush seal depend largely on the

eccentricity of the shaft. Bilal and Patrick. successfully analysed the chronological wear development of the clamped brush seal and investigated the blow-down effect and bristle stiffness under a super-heated steam environment [10]. The low inclined bristle of the tandem geometry presented a continuously increasing wear to the rotor and bristle tip surface and showed the performance influenced by the bristle pack design. The research on the sealing problems is of great significance in the design of turbines and aircraft engines, with the constant pursuit of high thrust ratio and low fuel consumption. Many experimental studies give information that the brush seal not only has good sealing characteristics, and high sealing efficiency but also has low manufacturing cost and a simple structure. The leakage of the brush seal is only 10%–20% of the same level as a labyrinth seal. The actual application shows that just using a brush seal instead of a traditional labyrinth seal at one or several critical parts can make the engine's thrust increase by 1%–3% and the fuel consumption decrease by 3%–5% according to Zhang et al [11]. Therefore, brush seals have great potential for improving engine performance.

3.2. Attachment of brush seals

In this study, the attachment of brush seals to the rotor-shaft was evaluated by the replacement of mechanical seals with the floating brush seal. In addition, an exploratory study that enhances sealing technology was undertaken by determining brush seal leakages by means of brush seal analysis. A brush seal contains many thousands of fine wires, which touch the rotor, forming an effective barrier to the steam flow, whilst retaining the ability to deflect during shaft excursions and thermal movements without permanent loss of sealing efficiency according to Chen et al [12].

The FBS is a combination of carbon seal and brush seal technology, enclosed in a lightweight stainless-steel band. Its purpose is to withstand condensate flashing and offer a reduced and more consistent leakage rate. Unlike other alternatives, the FBS can tolerate vibration, bearing failures, and radial movement better because it is a floating seal. The brush seal serves as the main shaft seal, facing high-pressure steam. It quickly reduces pressure and filters out steam impurities with its bristles to safeguard downstream carbon rings according to Zanini et

al [13]. The floating brush seal (FBS) acts as a face seal against the gland wall or separator plate downstream. It can easily replace a carbon ring, fitting into the same space. The seal is split into two segments that are held together by a garter spring. Its self-centering design may eliminate the need for complex alignment procedures in certain cases. Figure 4 displays an image of the floating brush seal, of which the explanatory diagrams for the attachment and split design can be found in the appendix section, under Figures A1, A2, and A4.

Figure 4. A floating brush seal (Pumps & systems).

4. Brush Seal Porous Media Model

Due to the dense arrangement of bristles, it is challenging to create a comprehensive numerical model for brush seals. Consequently, most simulations rely on equivalent porous media techniques. In this study, the analytical approach employed is known as the renormalization group (RNG) k–ε model with specific adjustments. This particular model takes into account both turbulent steam flow and rotational motion in the brush seal field, making it more precise than other models which only consider flow conditions. By incorporating spatial coordinate functions, this method offers improved accuracy in solving brush seal flows.

The porous media model method is utilized to incorporate both the viscous drag item and the inertia resistance item into the flow control equation. This involves determining αi, which represents the viscous drag coefficient, as well as βi, representing the inertial

drag coefficient in three orthogonal directions. These coefficients are interconnected with bristle bundle size parameter according to Equation 4 of simplified fluid control theory. Eugen's equations (5 and 6) demonstrate how to calculate these respective values for each type of drag coefficient effectively.

$$\frac{dp}{dx} = \left(\frac{P\alpha i}{2} \ /\mu_i \ / + \beta_i \ \mu\right); \qquad (4)$$

$$\alpha_i = \frac{7}{2d} \ \frac{(1-\varepsilon_{\alpha i})}{\varepsilon_{\alpha i}}; \qquad (5)$$

$$\beta_i = \frac{150}{d^2} \ \frac{(1-\varepsilon_{\alpha i})^2}{\varepsilon_{\alpha i}^3}; \qquad (6)$$

The values of αi and βi can be derived from the experimental data or determined using empirical formulas that directly correlate with the bristle diameter. The porosity of the porous medium surface, denoted as ɣαi (representing porosity in a section perpendicular to a specific direction), along with its counterparts in three directions, can be calculated by employing equations 7, 8 and 9.

Axial surface Porosity:

$$\varepsilon_{\alpha x} = 1 - \frac{d^2 n}{2(D_0 + D_1)Bcos\theta}; \qquad (7)$$

Radial Surface Porosity:

$$\varepsilon_{\alpha r} = 1 - \frac{d^2 n}{4DBcos\theta}; \ ; \qquad (8)$$

Peripheral Porosity:

$$\varepsilon_{\alpha o} = 1 - \frac{d^2 n}{2(D_0+D_1)Bcos\theta}; \qquad (9)$$

The size parameters, along with the values of n, D_0, D_i, and β are determined based on processing and assembly dimensions. The thickness B of the brush bundle uniquely determines the surface porosity $\varepsilon\alpha_i$ and subsequently dictates the values of α_i and β_i. However, determining the thickness B is not solely reliant on design parameters such as bristle diameter or quantity; it also depends on how they are arranged within their bundles.

When the bristle bundles are not in use, they are arranged loosely and have their maximum thickness. They also have the highest level of porosity. As the pressure difference between the inlet and outlet is increased, it compresses the bristles causing a change in value B. The greater this pressure difference becomes, the thinner it makes the bristle bundle and reduces its porosity. Eventually, there will be a minimum thickness reached by the brush bundle while further increasing pressure difference has no effect on its porosity anymore. These different arrangements can be seen in Figure 5 according to previous research studies where empirical parameters were used to determine bristle bundle thickness for d=0-5mm with Δp=0-1.5 MPa range situations.
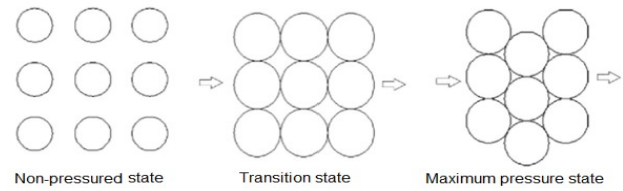

Figure 5. Brush arrangements in different pressure states.

Nonetheless, the effectiveness of this approach is compromised due to the uncertainties surrounding how bristle deformation impacts thickness. Consequently, we employed a two-way fluid-solid coupling model in our study to computationally evaluate alterations in shape and position of brush bristles during constant pressure difference operations. Subsequently, we determined brush bundle thickness and porosity by assessing these changes. By calculating the viscous drag coefficient and inertial drag coefficient through this process, key parameters for the porous media model can be established.

5. Results and Discussions

Circumferentially symmetric bristles are used in this study to simplify the analysis of a model with two rows and six columns using Ansys APDL. The size of the model can be seen in Figure 6. The brush material chosen for this model is a cobalt-based super alloy with an elasticity modulus of 225 kN/mm^2 and a Poisson's ratio of 0.3. In actual working conditions, the brush seal may experience blown-down effect due to factors such as

radial runout of the rotating shaft, excessive wear, and changes in working conditions. However, for this study, we will only consider the blow-down effect caused by the back baffle. Further analysis of this specific blow-down effect will be discussed below.
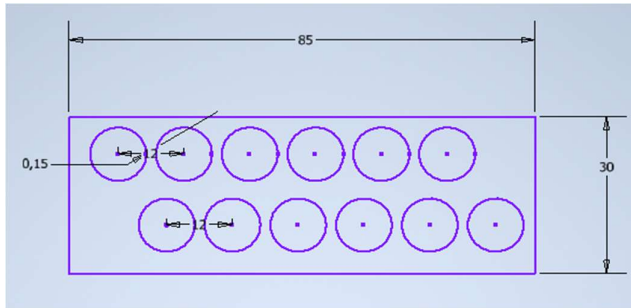

Figure 6. Simplified fluid-solid coupling model with dimensions.

This study found that when the calculated pressure is low, there is only minimal deformation of the bristle, and the back baffle protection height adequately prevents any significant influence on filament deformation. The actual amount of bristle deformations in fluid-solid coupling calculations depend on both the pressure ratio and back baffle protection height. To begin with, a solid model and a fluid model must be created together in Ansys Workbench for accurate modeling. Then, during meshing process, separate suppression of solid and fluid models should be applied to ensure reliable results. In order to prevent the occurrence of negative volume grids during mesh deformation caused by information exchange between the solid and fluid models on the coupling surface, tetrahedral cells are utilized in both the solid and fluid domains. The Reynolds number is an essential parameter extensively employed in fluid dynamics which can be readily calculated based on fluid properties and operating conditions. Additionally, it serves as a useful tool for evaluating flow regime. Nevertheless, when analyzing turbulent flow characteristics comprehensively, the k-epsilon turbulence model provides a more thorough analysis approach. The k-epsilon turbulence model is a mathematical representation used to describe and predict turbulent flows. It provides additional insights into the properties of turbulence. The Reynolds number, on the other hand, is not affected by the choice of turbulence model but helps determine the flow regime. By employing

the RNG k–ε turbulence model and setting boundary conditions such as inlet/outlet pressure and temperature, fluid-solid coupling surface, dynamic mesh parameters, time step size, and number of iterations we establish our calculation model in Ansys workbench as shown in Figure 7, and more of the calculation process can be found in the appendix section under Figure A3.
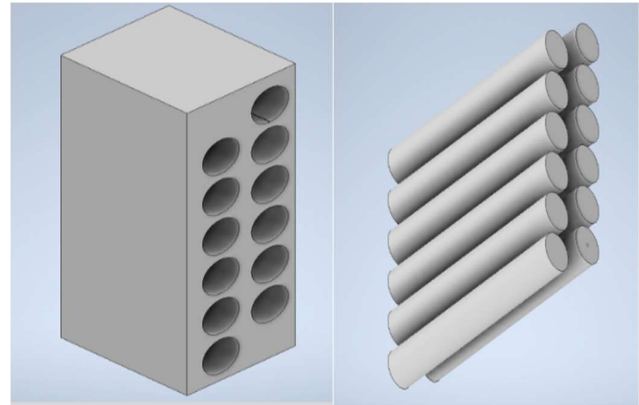

Figure 7. The calculation model.

The coupling surfaces in the fluid-solid system are made up of cylindrical surfaces around the circumference and wire-free ends. In the transient solver, these coupling surfaces are designated as system couplings. The circumferential wall of the flow field acts as a dynamic mesh area to move with the deformation motion of the coupling surface. The rotor surface is treated as a non-slip boundary condition on which no sliding occurs. To simulate changes in flow shape caused by movement at boundaries, we utilize a dynamic mesh model. For this analysis involving 219,729 elements in our mesh plot, we opted for using the k-epsilon turbulence model due to its turning point characteristics. Figure 8 and Figure 9 depicts both solid grids and fluid grids used in this simulation process.
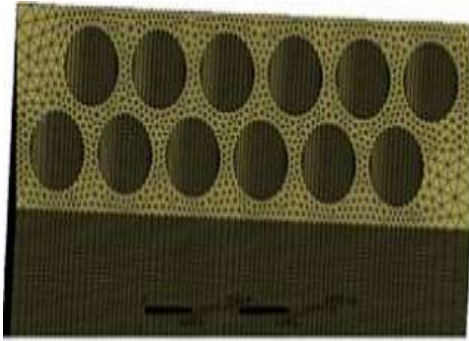

Figure 8. The solid grids.

Figure 9. The liquid grids.

uniform load, greater bending deformations occur with longer brushes.

Figure 10. Deformable brush at 1.0 s.

However, it is worth noting that the present fluid-solid coupling model can directly compute the leakage rate. It should be emphasized that determining the leakage rate for only two rows and six columns does not represent calculating it for the entire encounter ring. Data are incorporated into the encounter ring when there is a significant number of encounter rows in its structure.

The study employs both a fluid-solid coupling model and a porous media model to determine the extent of distortion encountered. This calculated data is then incorporated into the new porous medium model once convergence is achieved in the fluid-solid coupling model. Consequently, this determines the sealing properties of encounter seals amidst encountered distortion conditions.
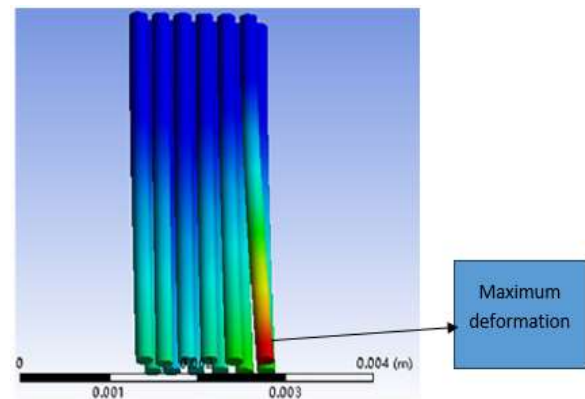
In Figure 11, the deformation of the brush wire can be observed from a bottom view perspective. The original position of the brush is depicted by the transparent cylinder. This deformation measures roughly half of the brush wire's diameter and reaches its maximum at the back plate exit point. Consequently, this deformity affects the thickness of the brush itself. As a result, it should be noted that there exists variability in both numerical analysis and experimental evaluation when determining this value for bundle deformation. This fluctuation arises due to steam flow impact on an ongoing basis. Figure 12 illustrates one such instance where clear cut deformities are visible within a calculated timeframe spanning from start to finish over 1 second.
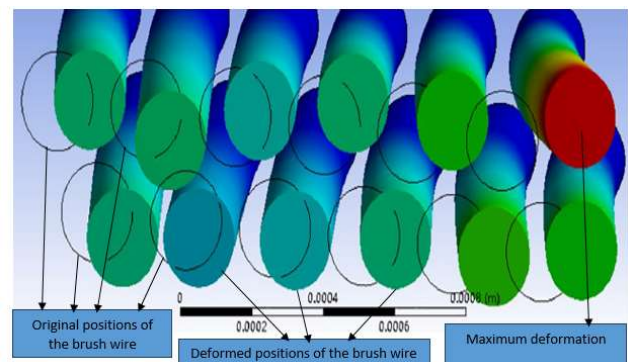
5.1. Solid analysis of brush seal

To determine the bristle deformation parameters, an analysis is conducted on the solid part. The solid brush component is treated as a transient problem due to its simplified model selection. It should be noted that a single amount of deformation can affect the entire brush, while synthetic analysis of wire deformation in the brush can only be done over the entire calculation period. After 1.0 s of iteration time, deformation results for the complete solid computing domain are evaluated and depicted in Figure 10. This figure clearly illustrates the deformation of the brush wire, which primarily occurs in the lower section of the brush and exhibits maximum bending near its contact surface at the outlet. Like a fixed end in a cantilever beam model, the top part of the brush remains stationary while becoming progressively closer to its bottom as length increases. Consequently, under a

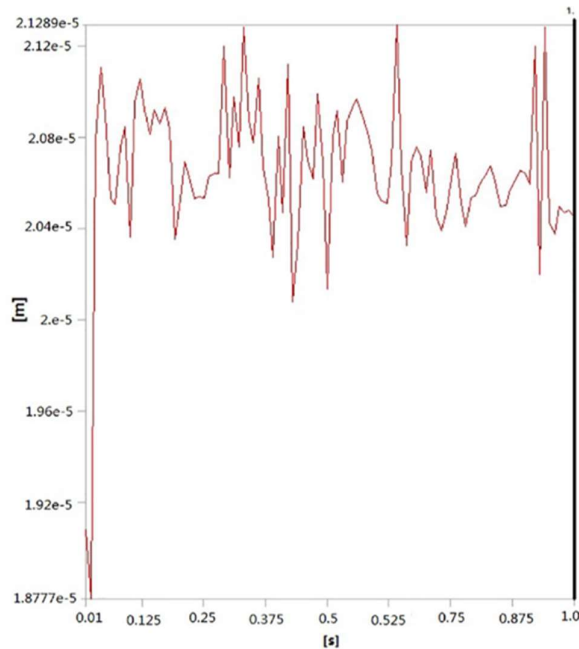**Figure 11.** Deformable brush at 1.0 s bottom view.

Figure 12. The maximum amount of deformation of a single brush during 1.0s.

The calculation period is divided into two stages. In the first stage, known as loading pressure, the bristle experiences rapid deformation due to initial space in the brush. As pressure is applied and the space compresses, the bundle deforms accordingly. Figure 12 demonstrates this initial deformity with a steep gradient curve. Due to steam flow instability and elasticity of both steam and brush material, when medium flows through it will exert force on the brush bundle resulting in stored energy in elastic potential form within said bundle. Once enough potential energy is gathered during the initial stage, it will result in instability during the second stage. This leads to a relatively stable deformation of the brush bristles which characterizes this subsequent phase. Despite its unstable nature, the deformation of these second-stage bristles oscillates around a constant value known as their average deformation level. Hence, determining and evaluating this mean deformity becomes feasible for calculating purposes involving wire brushes in such stages.

5.2. Liquid analysis of brush seal

To observe the distribution of physical quantities across a brush wire, it is important to establish its cross-section. Figure 13 displays the velocity streamlines and

vectors of the flow field, indicating that at the steam outlet, there is maximum speed in line with findings from other studies. This phenomenon occurs due to a sudden decrease in cross-section leading to pressure reduction; subsequently causing an increase in speed which becomes a major cause of leakage. This observation can be better visualized through Figure 13 and Figure 14 depicting a cloud picture without brush wire present.
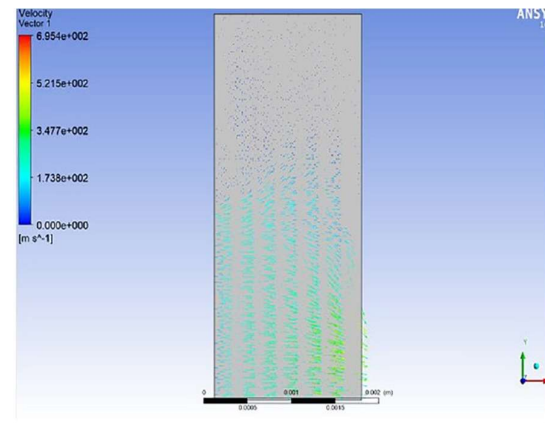

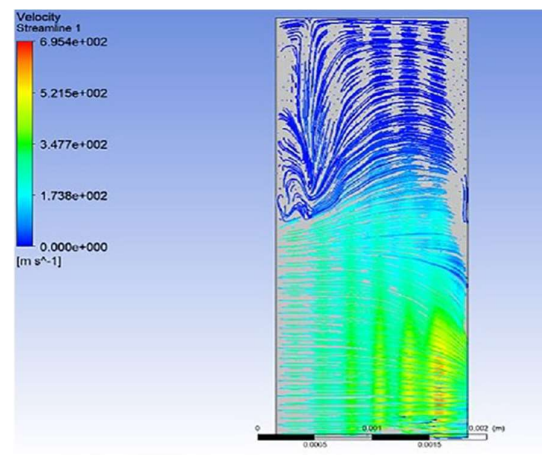**Figure 13.** Local magnification velocity vector.

Figure 14. Velocity streamline.

Furthermore, a thorough analysis of the pressure field is conducted to confirm that there are no alterations in the two sections mentioned previously. Figure 15 presents an illustration of the pressure cloud image. The overall behavior of the pressure field within the brush can be examined through Figure 15 as well. Not accounting for any positional effects on its performance, it becomes

evident that the distribution pattern of pressures maintains consistency with those observed in previous models encompassing porous materials: namely, gradual decrease from left to right and concentration primarily at lower regions within bristles; this coincides with maximum gradient found near back plate gaps due to disparities resulting from constructional features such as back baffles which cause radial differences in pressure across brush seals creating a blow-down effect.

Additionally, the calculations using fluid-solid coupling methods consider the deformations caused by the specific characteristics of the bristle arrangement. This ensures a thorough analysis is conducted for every aspect involved, including the straight-line segment that covers the entire bundle of brushes.
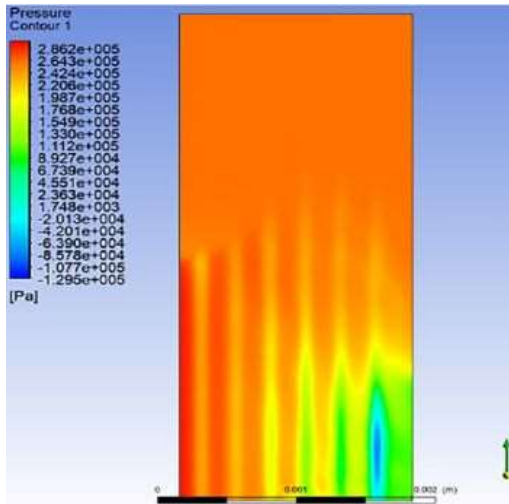

Figure 15. Pressure cloud picture

6. Brush Seal Fluid-Solid Coupling Analysis

The solid component and the fluid component are computed independently, and their data is then shared and exchanged to derive the final calculation result. This process is depicted in Figure 16.

The combination of the fluid-solid coupling model and the porous medium model is required to accurately calculate the leakage in the brush ring. The exact impact of the number of filaments on leakage cannot be determined solely using the fluid-solid coupling model. In this combined approach, it is crucial to incorporate feedback on bristle deformation.
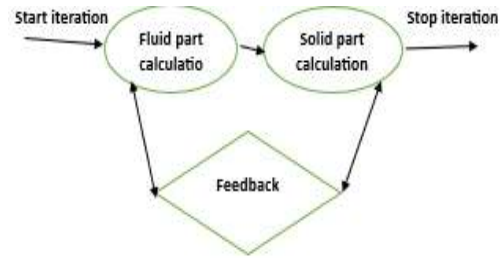

Figure 16. A flowchart of the fluid–solid coupling calculation process [14].

The previous study on the porous medium model concluded that steam flow in the brush is mainly concentrated at the height of half of a brush wire. To represent this deformation, an average deformation value of 0.2 mm for the brush was established. However, it is necessary to calculate changes in the coefficient of porous media based on Eugen's Equations (5) and (6), as well as consider porosity levels. The porosity level in the brush depends solely on its thickness B after determining geometric parameters for bristle placement. The change pattern for B values can be analyzed numerically using fluid-solid coupling analysis methods. To determine both porosity and resistance coefficients under various pressure differences, Equations 10 through 13 proposed by Yue et al, Yue C, Bitian S and Lanzhu Z, are employed during calculations process [15], [16].

Porosity after deformation:

$$\varepsilon = 1 - \frac{d^2\, n(D_0 - D_1)}{2(D_0^2 - D_1^2)\, B cos\theta}\; ; \tag{10}$$

Viscous resistance coefficient:

$$\alpha_n = 80\frac{(1-\varepsilon)^2}{\varepsilon^3\, d^2}\; ; \tag{11}$$

$$\alpha_z = \alpha_n, \alpha_s = 32\frac{(1-\varepsilon)^2}{\varepsilon^3\, d^2} \tag{12}$$

Initial resistance coefficient:

$$\beta_n = 1.16\frac{1-\varepsilon}{\varepsilon^2\, d}\; ; \tag{13}$$

$$\beta_z = \beta_n, \beta_s = 0,; \tag{14}$$

Table 2. Calculation of the leakage values.

Δp (MPa)	Deformation (mm)	Porosity	Leakage without deformation (kg/s)	Leakage with deformation (kg/s)	Leakage decreasing with deformation (%)
0.2	0.12	0.602	0.156	0.143	1.3
0.3	0.126	0.600	0.198	0.175	2.3
0.4	0.13	0.598	0.221	0.201	2

The research team conducted a fluid analysis of porous media using a steady-state model. They considered parameters related to viscous resistance and inertia resistance before and after brush deformation. These coefficients were defined in fluent, with their expressions represented by space vectors. The entire brush ring was symmetric along the center axis.

Table 2 displays the results obtained from calculations performed at different pressure differences. The second column shows the average deformation of the filament after considering fluid-solid coupling during calculation. The third column presents porosity values calculated using Equation 10. Finally, the table illustrates leakage calculation results under two conditions: without any deformations and with deformations considered. The final column denotes the difference between these two cases.

7. Conclusion

The numerical analysis of the brush seal is conducted using a practical engineering approach. However, due to experimental limitations, we had to refer to previous experiments for obtaining the size and operating parameters of the simulated brush seal ring in this project. We compare the leakage rate data obtained from our brush seal leakage test with simulation data gathered earlier from our two-way rotating dynamic seal experimental device, thus illustrating their variation pattern. The comparison chart can be found in the appendix section under Figure A5.

The simulation results in the appendix section under Figure A5 closely align with the experimental data, indicating reliable and accurate prediction. The observed trend indicates that leakage increases as the pressure difference increases. It is worth noting that considering the deformation of the brush wire leads to a more accurate representation of leakage in relation to actual experiments

conducted at different examination points. Therefore, it can be concluded that combining the modified porous media model and fluid-solid coupling model provides a closer estimation of brush seal leakages when compared to reality. Regarding the efficiency of the turbine, it is proven that brush seals are an effective means of improving steam turbine efficiency. However, the following conclusions can be drawn:

- Brush seals provide significant performance benefits in overall heat rate due to reduced leakage rates for utility steam turbines (the actual benefit is application-specific).
- Brush seal design characteristics are well understood.
- Consideration of the turbine as a system is important for the full performance benefit of brush seals to be realised.
- Brush seal quality is essential to maximising performance benefits.
- Effective clearance calculations have been expressed for both choked and unchoked flow. It was applied to compare the brush seal leakage performance for different cases and geometries.
- Rotor interference, fence height, cant angle, and bristle diameter have a strong influence on brush porosity and leakage performance since they affect the fluid velocity profile and flow behaviour.
- The larger the thickness of the brush, the smaller the leakage, and the better the sealing performance.
- The leakage flow of the brush seal increases with the increase of pressure difference.
- The pressure in the brush is gradually reduced in the direction of the axial direction and the maximum pressure gradient occurs at the exit of the back plate.

- Among the various approaches to model brush seal leakage flow, porous medium modelling of the bristle pack provides the most insight to assist designers.
- The CAE methodologies developed in this study and their correlation with the test data give insight for the physics under turbine operating conditions. Further analyses will be useful for estimating frictional heat generation and resulting effects on rotor durability and dynamics.

These results were compared with that of other researchers with other approaches of different technical aspects, like the Numerical Investigation on the Leakage Characteristics of Brush Seals Based on Fluid-Structure Interaction which was presented at the 7th International Conference on Education, Management, Computer and Society (EMCS 2017) by Yitong Wang from the School of Civil Engineering, University of Science and Technology LiaoNing, Anshan 114051 China. Yitong Wang investigated the leakage characteristics of Brush using two-way FSI and the results were compared with the experimental data, the comparison plot is shown in the appendix section under Figure A6. Moreover, our data plot analysis of brush seals which can be found in the appendix section under Figure A5 appears to align with the findings of Yitong Wang, despite differences in the technical approach employed. This suggests that our results may be robust across varying methodologies, enhancing the reliability of our conclusions.

Nomenclature

Abbreviations and Description:

APDL	Ansys parametric design language
ANSYS	Analysis system
BCs	Boundary conditions
BH	Bristle height
CAD	Computer-aided design
CAE	Computer-aided engineering
CFD	Computational fluid dynamics
DOF	Degree of freedom

FBS	Floating brush seal
FEA	Finite element analysis
FEM	Finite element method
FH	Fence height
FS1	Fluid-structure interaction
HP	High pressure

Acknowledgement

Competing Interest Statement

The authors declare no known competing financial interests or personal relationships that could have influenced the work reported in this paper.

Data and Materials Accessibility

No additional data or materials were utilized for the research described in the article.

Funding

Reference

[1] B. Qiu, J. Li, and X. Yan, "Investigation into the flow behavior of multi-stage brush seals," *Proc. Inst. Mech. Eng. Part A: J. Power Energy,* vol. 228, no. 4, pp. 416-428, 2014, doi: 10.1016/10.1177/0957650914522456.

[2] D. Ma, J. Li, Y. Zhang, Z. Li, X. Yan, and L. Song, "Application of blade tip shroud brush seal to improve the aerodynamic performance of turbine stage," *Proc. Inst. Mech. Eng. Part A: J. Power Energy,* vol. 234, no. 6, pp. 777-794, 2020, doi: 10.1177/0957650919883153.

[3] J. Zhang, M. Liu, and N. Peng, "Study of Heat Transfer and Leakage Characteristics of Brush Seals Based on Local

Temperature Non-Equilibrium Model," *Machines,* vol. 10, no. 9, p. 823, 2022, doi: 10.3390/machines10090823.

[4] M. Hildebrandt, H. Schwarz, C. Schwitzke, H.-J. Bauer, and J. Friedrichs, "Effects of the Back Plate Inner Diameter on the Frictional Heat Input and General Performance of Brush Seals," *Aerospace,* vol. 5, no. 2, p. 58, 2018, doi: 10.3390/aerospace5020058.

[5] J. W. Chew and S. Hogg, "Porosity Modeling of Brush Seals," *Journal of Tribology-Transactions of The ASME*, vol. 119, pp. 769-775, 1997, doi: 10.1115/1.2833883.

[6] Y. Liu, B. Yue, X. Kong, H. Chen, and H. Lu, "Effects of Front Plate Geometry on Brush Seal in Highly Swirling Environments of Gas Turbine," *Energies*, vol. 14, no. 22, p. 7768, 2021, doi: 10.3390/en14227768.

[7] Z. Yuanqiao, D. Ma, J. Li, Y. He, J. Ji, B. Sun, Z. Li, and X. Yan, "Effect of the Fence Height on the Leakage Flow Characteristics of Brush Seals," Sep. 2019, doi: 10.33737/gpps19-bj-021.

[8] P. Reggentin and J. Friedrichs, "Investigation of Brush Seal Instabilities," in *Proceedings of the ASME Turbo Expo 2020: Turbomachinery Technical Conference and Exposition,* GT2020-3514, 2020, doi: 10.2514/6.2020-3514.

[9] Y. Ha, T.-W. Ha, J. Byun, and Y. Lee, "Estimation of the rotordynamic characteristics of a single brush seal using least-squares and instrumental variable methods under super-heated steam environment," *Adv. Mech. Eng.,* vol. 12, no. 3, pp. 1-13, 2020, doi: 10.1177/1687814020913676.

[10] B. Outirba and P. Hendrick, "Experimental characterization of friction and heat generation of carbon fibre brush seals for aero-engines," *Tribol. Int.,* vol. 151, p. 106448, 2020, doi: 10.1016/j.triboint.2020.106448.

[11] J. Zhang, M. Liu, and N. Peng, "Study of Heat Transfer and Leakage Characteristics of Brush Seals Based on Local Temperature Non-Equilibrium Model," *Machines,* vol. 10, no. 9, p. 823, 2022, doi: 10.1016/10.3390/machines10090823.

[12] L. Chen, P. Wood, T. Jones, and J. Chew, "Detailed Experimental Studies of Flow in Large Scale Brush Seal Model and a Comparison with CFD Predictions," J. Eng. Gas Turb. Power, vol. 122, no. 3, pp. 10-17, 2000, doi: 10.1115/1.1287265.

[13] P. Zanini, J. Kim, J. Sandridge, and B. Gilmore Jr., "Improving Reliability and Reducing Steam Leakage in General Purpose Steam Turbines with Floating Brush Seals," *Turbomachinery Laboratories, Texas A&M Engineering Experiment Station,* 2016. [Online]. Available: https://hdl.handle.net/1969.1/159777.

[14] B. H. Lodhia and S. R. Clark, "Computation of vertical fluid mobility of CO, methane, hydrogen and hydrocarbons through sandstones and carbonates," *Sci Rep*, vol. 12, p. 10216, 2022, doi: doi.org/10.1038/s41598-022-14234-6.

[15] C. Yue, S. Bitian, and Z. Lanzhu, "Leakage performance predictions of a brush seal based on fluid–solid coupling method," *Sci. Prog.,* vol. 103, no. 2, pp. 1-16, 2020, doi: 10.1177/0036850419897221.

[16] C. Yue, S. Bitian, and Z. Lanzhu, "Leakage performance predictions of a brush seal based on fluid–solid coupling method," *Sci. Prog.,* vol. 103, no. 1, pp. 1-16, 2020, doi: 10.1177/0036850419897221.

[17] Y. Wang, "Numerical Investigation on the Leakage Characteristics of Brush Seals Based on Fluid-Structure Interaction," in *Proceedings of the 2017 7th International Conference on Education, Management, Computer and Society (EMCS 2017)*, Atlantis Press, 2017, pp. 210-216, doi: 10.2991/emcs-17.2017.42.
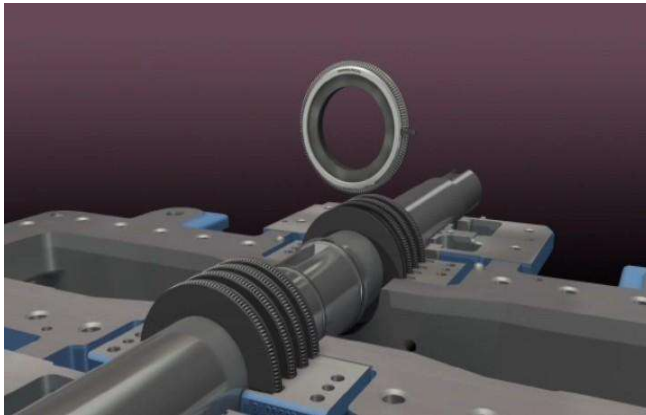
Appendix

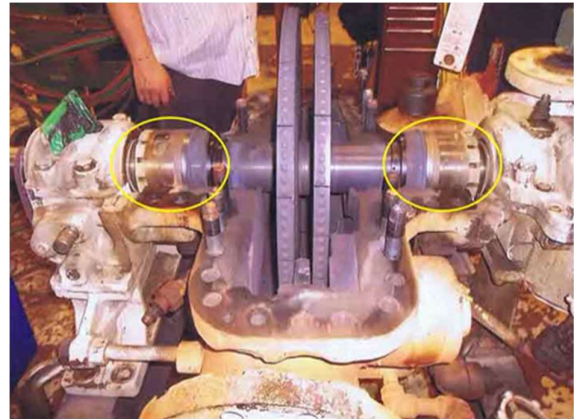**Figure A1.** Floating Brush ring to be attached in place of the mechanical seal (Inpro/Seal).

Figure A4. Mechanical seal to be replaced with Brush seal (Inpro/Seal).

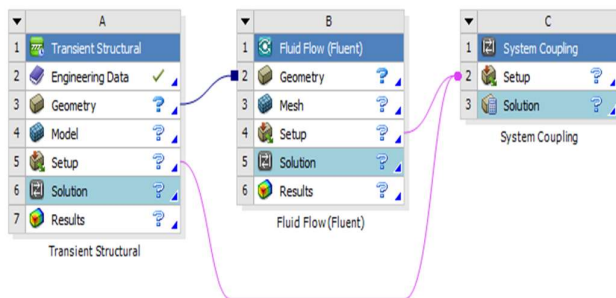**Figure A2.** Split design shown (Inpro/Seal).

Figure A5. The data contrast.

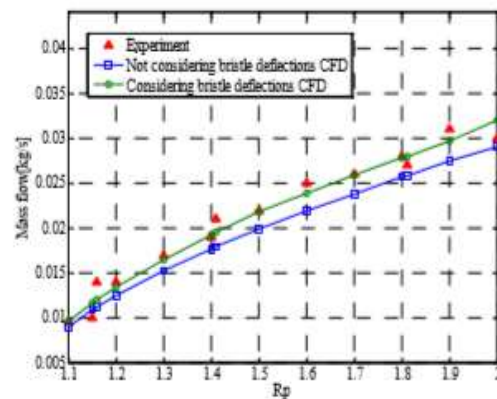**Figure A3.** Fluid-Solid coupling model (Ansys workbench).

Figure A6. Comparison of experimental leakage with CFD [17].